3D LCS Proof of Concept for Sea Breeze

Greg Seroka, Erick Fredj, and Rich Dunk
AquaWind, LLC
March 2021

1. INTRODUCTION

Seroka et al. (2018) studied two pure sea breezes in New Jersey that occurred in 2012 and 2013. By using the new to sea breeze Lagrangian method called relative dispersion (RD), the authors were able to clarify the sea breeze circulation both onshore and offshore, and quantify the sea breeze sensitivity to synoptic flow and upwelling. This was a proof of concept study, to test how relative dispersion calculations in two dimensions (2D) would enable better understanding of the sea breeze circulation.

Seroka et al. (2019) then extended this method from just the pure sea breeze to also the other three sea breeze types: corkscrew, backdoor, and synoptic. Finally, the National Renewable Energy Laboratory (NREL) completed assessment of the Rutgers University-Weather Research and Forecasting (RU-WRF) model, providing several recommendations to improve RU-WRF (Optis et al. 2020). These recommendations were used to update RU-WRF, and in turn Seroka et al. (2020) updated the WRF configuration used in these Lagrangian studies to closely match the RU-WRF configuration. Seroka et al. (2020) then ran this updated WRF configuration on the same 4 sea breeze cases, and then subsequently ran the same 2D RD calculations. This enabled direct comparison between the previous and updated WRF configurations.

All of the previous studies have employed 2D Lagrangian methods to study the sea breeze. Here, we would like to outline a proof of concept for using three-dimensional (3D) Lagrangian methods to study the sea breeze.

2. METHODS

Please see the previous Seroka et al. studies (2018, 2019, and 2020) for details of the WRF, trajectory, and RD calculation methodology. Below are the outlined steps we took for this 3D RD proof of concept for sea breeze:

1. Choose the synoptic sea breeze case (Aug 4 2017)
2. Run WRF on synoptic sea breeze case
    a. Same setup as Seroka et al. (2020) (NARR, RTG HR SST, same resolution, same WRF version 4.1.2)
3. Place particles on “seeding grid” within the 3km WRF wind field (same as for 2D)
    a. Horizontally: for 3D, particles are placed 10 km apart in the x- and y-directions (same as for 2D)
    b. Vertically:
        i. For 3D, vertical levels are at 50, 100, 150, 200, 250, 300, 350, 400… up to 2500 m

(For 2D, vertical levels were at 10, 50, 100, 150, 500, 600, 700, 800, 900, 1000, 1500, 2000, and 2500 m)

   c. For 3D LCS, there are 352,000 virtual passive particles in total that are initially seeded.

4. Run trajectories
   a. Once particles are seeded, particles are advected by the horizontal and vertical wind components every 10 minutes over 1 hour (1 hour "simulations") (same as 2D)
   b. The particles were tracked by a 3D Lagrangian Particle Model simulation tool adapted by Fredj in 2020 using the LAGRANTO analysis tool (Sprenger and Wernli, 2015).
5. Run 3D LCS RD calculation
   a. 3D RD is calculated at each spatial point by taking the mean distance between the particle released at a point and its two nearest neighbors in each direction (for a total of 6 nearest neighbors) after each 1-hr simulation.
   b. For 2D RD, it was the same but only the 4 nearest neighbors were considered as there were only 2 directions: east-west and north-south.
   c. As before, RD minus the initial separation distance of the particles was used in the figures. This represents the mean rate of separation of particles relative to the initial separation distance, and provides a speed (km/hr) of divergence and convergence.
6. Plot planar view maps of RD
   a. Same methods for 3D as for 2D
7. Take cross section and plot Hovmöller diagrams
   a. Same methods for 3D as for 2D

3. RESULTS

Vertical winds cause horizontal dispersion among the massless particles at different elevations. To highlight the evidence of vertical effects, we plotted trajectories of five individual particles. These particle trajectories are shown in Figures 1-5.

Seroka et al (2018) limited calculations to 2D trajectories due to the assumption that vertical velocities were *O*(100) times smaller than horizontal velocities during the sea breeze cases analyzed. These figures show some evidence that this initial assumption may need to be revisited; for example, Figure 2 shows *O*(100 m) of vertical motion with relatively little—*O*(1 km)—horizontal motion.

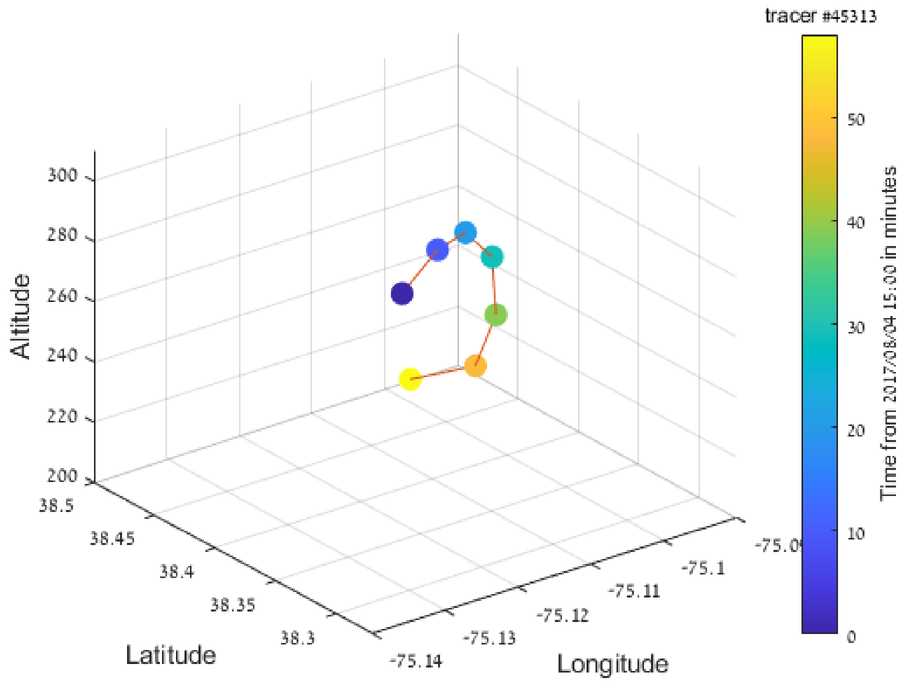

Figure 1. Sample particle #45313 to show vertical and horizontal movement over 1 hour.

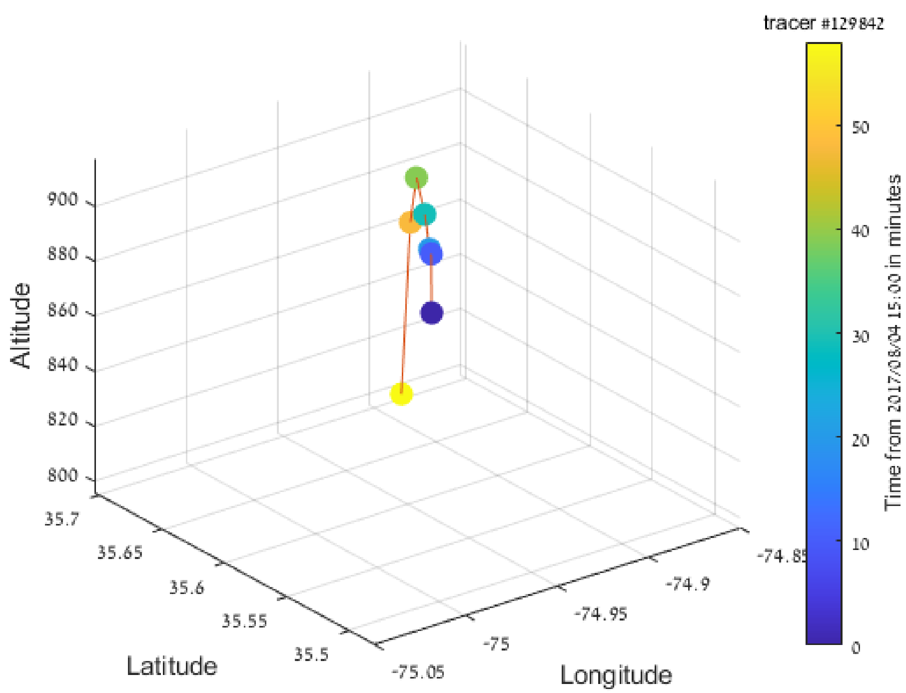

Figure 2. Sample particle #129842 to show vertical and horizontal movement over 1 hour.

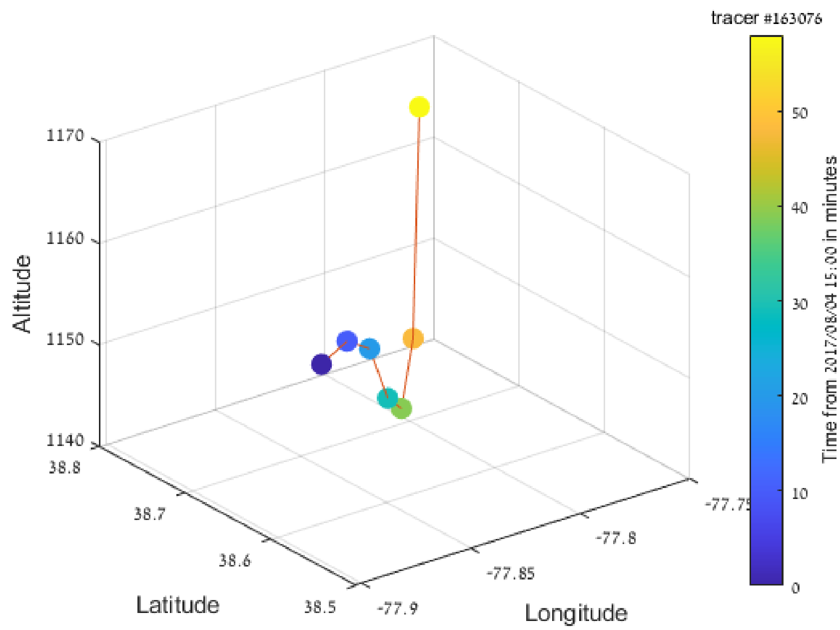

Figure 3. Sample particle #163076 to show vertical and horizontal movement over 1 hour.

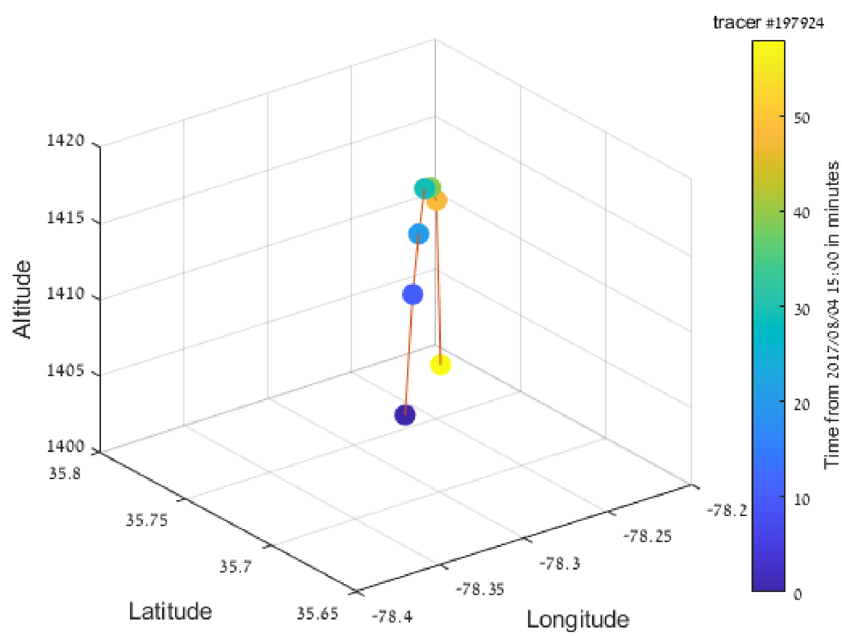

Figure 4. Sample particle #197924 to show vertical and horizontal movement over 1 hour.

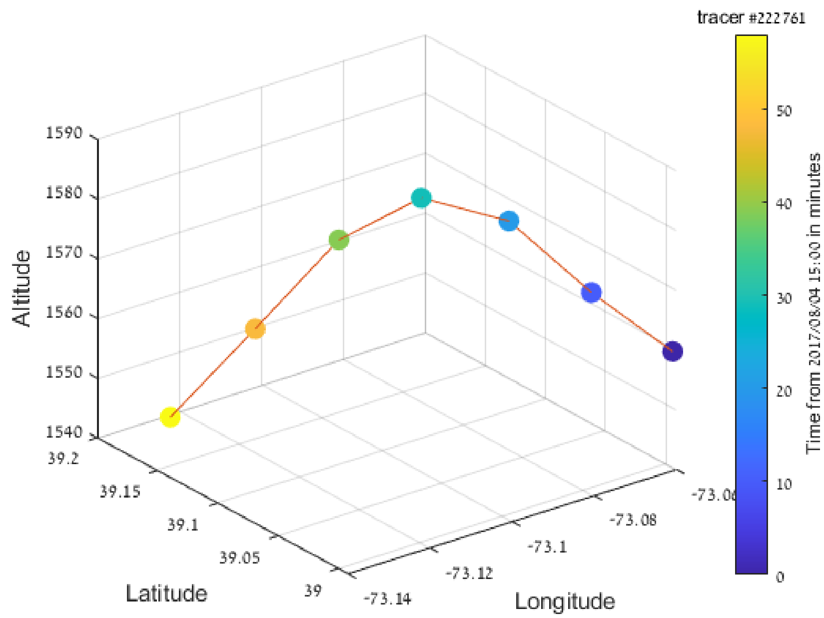

Figure 5. Sample particle #222761 to show vertical and horizontal movement over 1 hour.

To show the evolution of 3D RD in time and space, a series of 3 planar view maps of 3D RD was plotted. Each map shows the 3D RD at one time during the sea breeze and at one height. This was done in the same way as was done for 2D RD.

Figures 6, 7, and 8 show the map of 2D RD at 100 m (approximate wind turbine hub height) on Aug 4, 2017 at 1500, 2000, and 2300 UTC, respectively. These times were during the peak of the sea breeze circulation. To note, we now have the flexibility using newly developed software to choose the vertical height at which we plot the maps of 3D RD.

These figures show a very similar evolution of RD to the findings of Seroka et al (2020) for the synoptic sea breeze. Initially at 1500 UTC, general divergence occurs onshore and offshore with slightly higher divergence offshore and in Delaware Bay. Then at 2000 UTC an overall increase occurs in divergence everywhere with noisiness inland of a line between New York City and Philadelphia. Finally at 2300 UTC, even greater divergence everywhere occurs, and the front is fairly stationary or slightly inland of its position at 2000 UTC—just inshore of the NYC to Philadelphia line. In general, there seems to be larger divergence values with the 3D RD calculation, especially apparent at 2300 UTC (Figure 8) when compared to the same time and location in the previous 2D RD calculations.

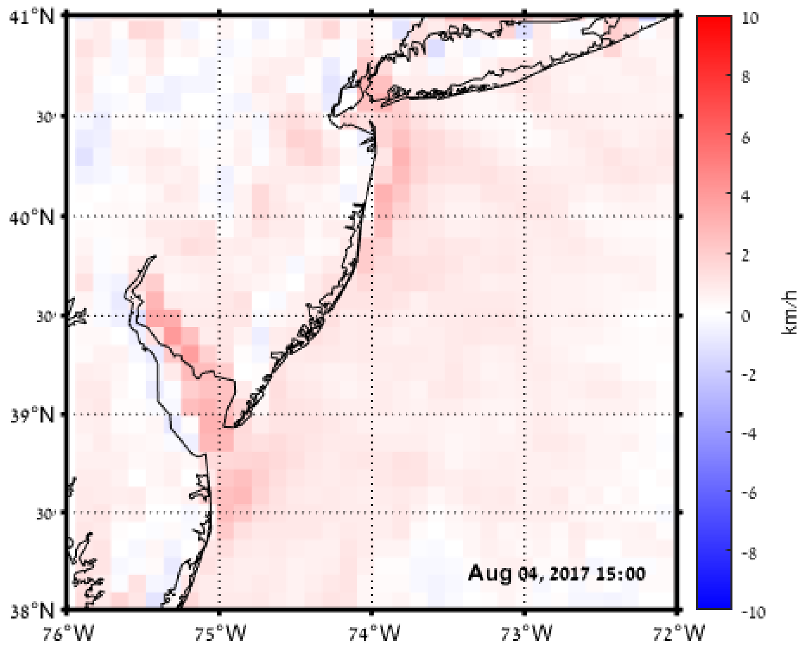

Figure 6. Shaded RD minus initial separation distance (km/hr) at 100 m at 1500 UTC on August 4, 2017. RD is from WRF/3D trajectory calculations. Red shading indicates divergence and blue shading indicates convergence in the Lagrangian wind field.

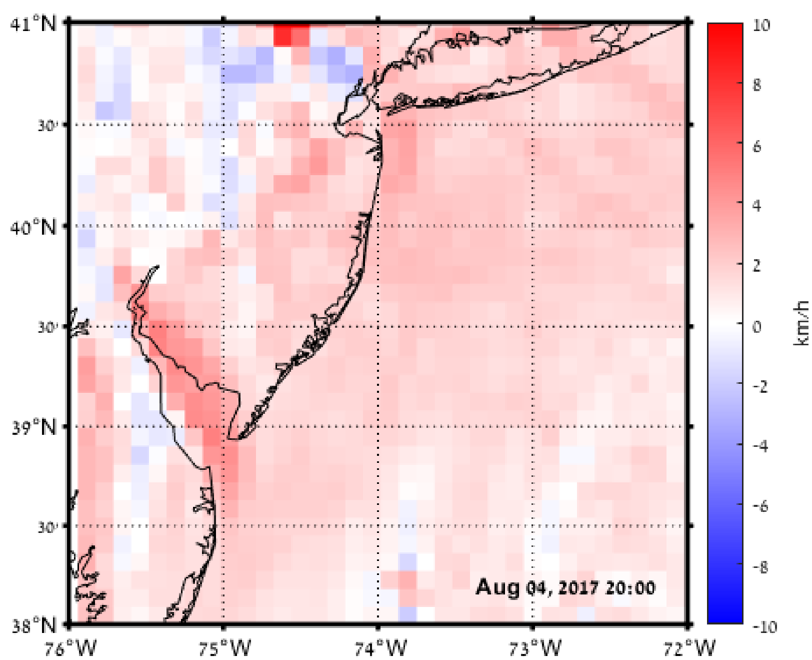

Figure 7. Same as Figure 6 but at 2000 UTC.

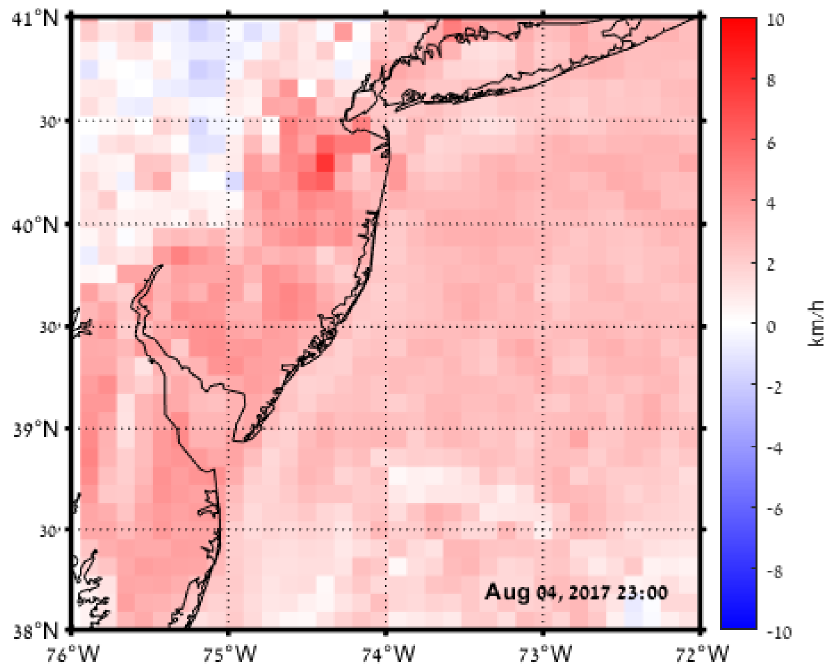

Figure 8. Same as Figure 6 but at 2300 UTC.

Next, maps of the cross section locations for the New Jersey and Maryland Hovmöller diagrams are shown (Figures 9 and 10). These are the same exact cross section locations as performed previously for the 2D RD calculations. Our newly developed software is also generic and flexible to produce the cross sections and Hovmöller diagrams quickly and on the fly, using an external CSV file.

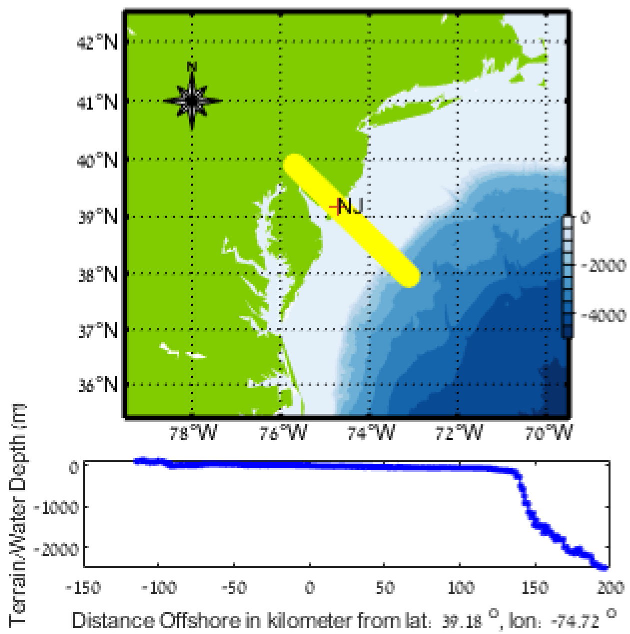

Figure 9. Location of the cross section performed for New Jersey, with terrain and water depth along the cross section depicted in blue at the bottom.

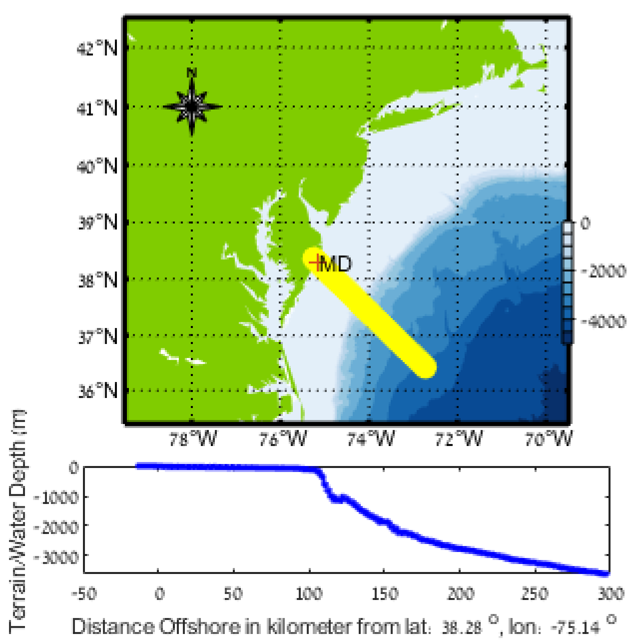

Figure 10. Same as Figure 9 but for the Maryland cross section.

Finally, Hovmöller diagrams (Figures 11-14) are shown for the cross sections for New Jersey and Maryland (Figures 9 and 10), at 100 m and 500 m heights, and at 00 to 09 UTC on August 4, 2017, prior to sea breeze formation and potentially during land breeze circulation from the previous day. Again, the newly developed software is generic and flexible and can produce the Hovmöller diagrams efficiently and on the fly.

Although these Hovmöller diagrams are shown as a proof of concept and so are not during the synoptic sea breeze circulation, they do show some interesting things. Figures 13 and 14 show an area of divergence and adjacent convergence at about 250 and 200 km offshore, respectively, at 01 UTC, with both propagating closer to the coast until about 05 UTC when the area of divergence dissipates at around 125 km offshore. The area of convergence continues propagating towards the coast until about 08 UTC when that dissipates at around 50 km offshore. Our previous studies showed via the Hovmöller diagrams that the sea breeze circulation cell expands and the divergence area propagates offshore with time. In this study, these Hovmöllers show that during the potential land breeze circulation, the divergence/convergence areas propagate onshore with time as the land breeze progresses with time.

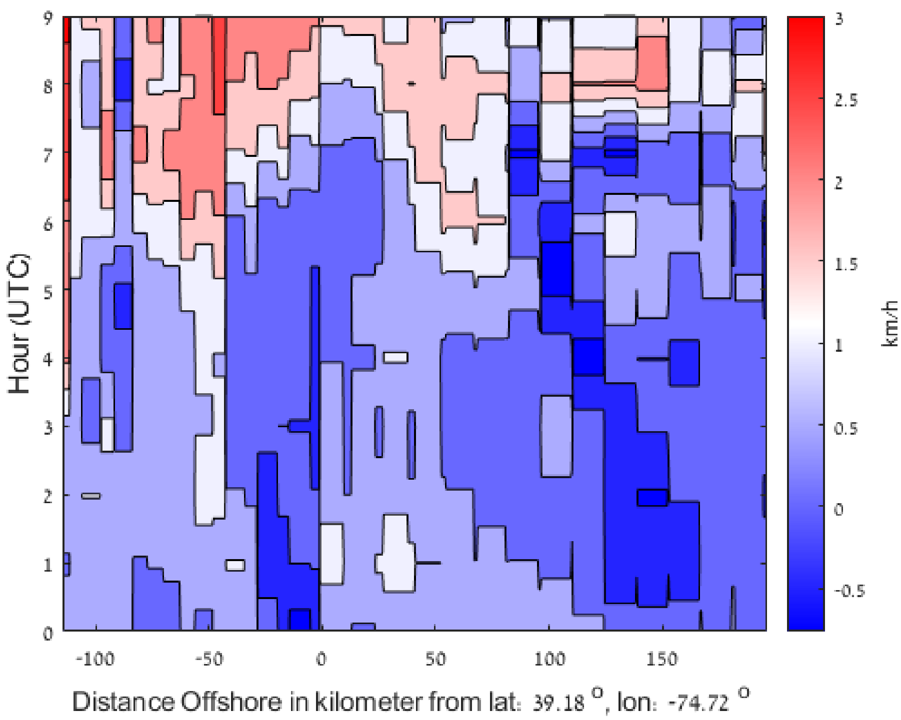

Figure 11. Hovmöller diagram of RD minus the initial separation distance at 100 m for the New Jersey cross section on August 4, 2017.

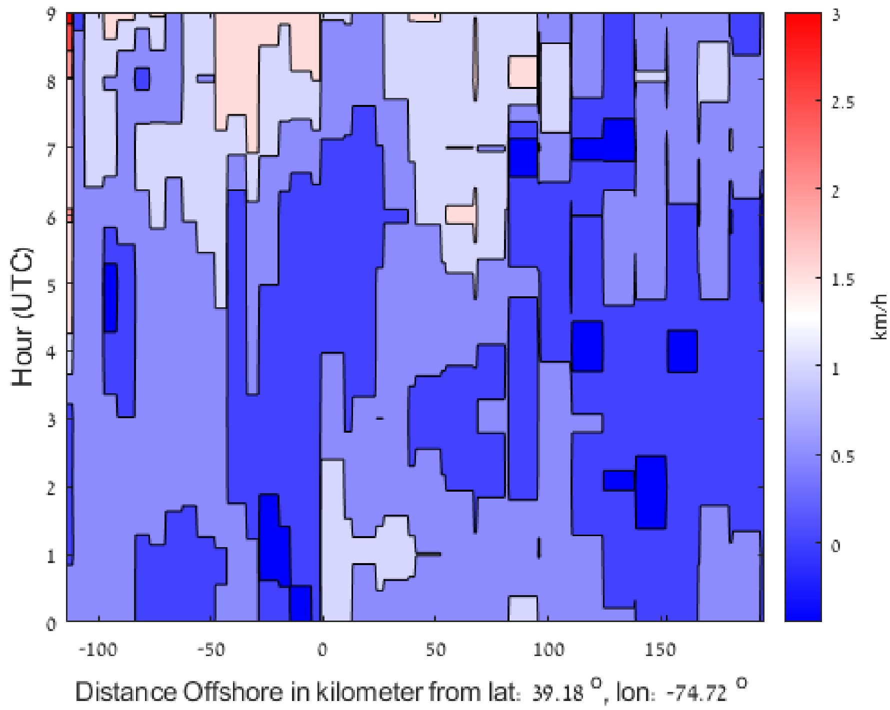

Figure 12. Same as Figure 11 but at 500 m for the New Jersey cross section.

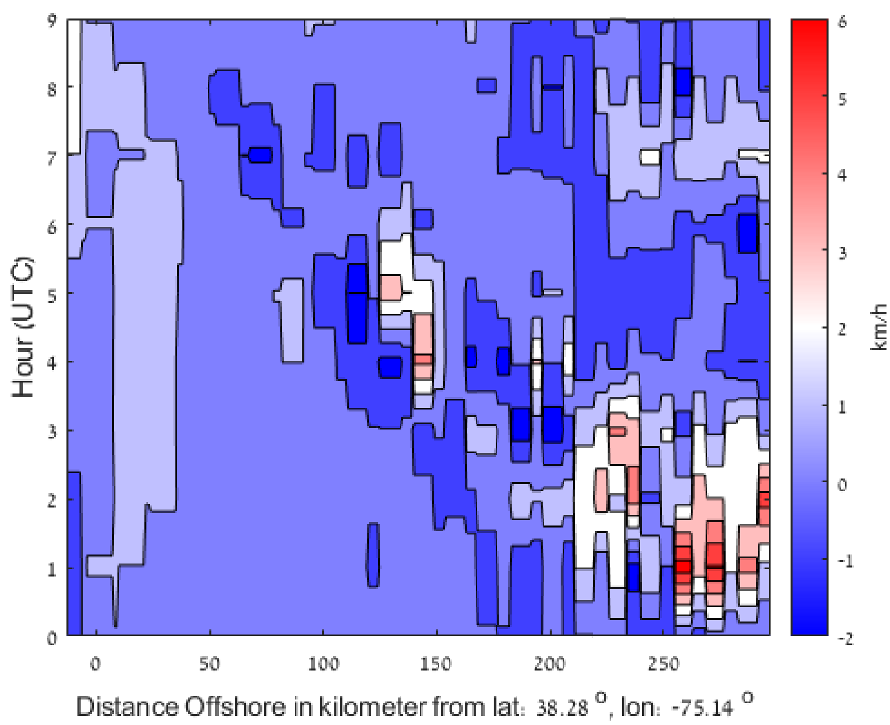

Figure 13. Same as Figure 11 but at 100 m for the Maryland cross section.

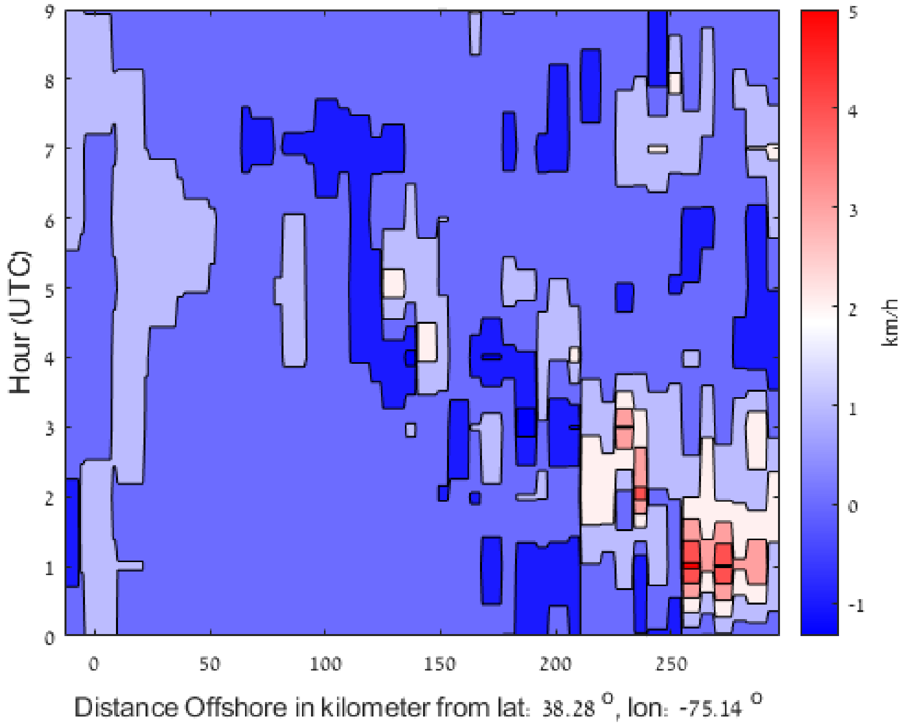

Figure 14. Same as Figure 11 but at 500 m for the Maryland cross section.

4. CONCLUSIONS

This study here provides a proof of concept methodology for calculating 3D relative dispersion using WRF wind fields to analyze the sea/land breeze circulation. The steps include choosing a sea breeze case study, running WRF, seeding particles and running trajectories on those particles, calculating the RD in three dimensions, plotting planar view maps of the RD, and finally taking cross sections and plotting Hovmöller diagrams. A few interesting items arose: 1) that vertical motions may be significant during the sea/land breeze circulation, 2) that divergence in RD may be larger when calculated in 3D than in 2D, and 3) that the land breeze component may be useful to compare to the sea breeze component—information that could be valuable for offshore wind development and resource assessment.

Ongoing work involves running the 3D RD calculations for all four types of sea breezes (pure, corkscrew, backdoor, and synoptic), direct comparisons between 2D and 3D RD calculations to challenge the vertical motion assumption, and analysis of both the sea and land breeze circulation components important for offshore wind resource characterization. Finally, wind turbine parameterizations available in WRF will be utilized to investigate wake effects from hypothetical wind turbine configurations, in both the Eulerian frame (wind vector fields) and Lagrangian frame (LCS/RD calculations).

5. REFERENCES

Optis, Mike, Andrew Kumler, George Scott, Mithu Debnath, and Pat Moriarty (2020). Validation of RU-WRF, the Custom Atmospheric Mesoscale Model of the Rutgers Center for Ocean Observing Leadership. Golden, CO: National Renewable Energy Laboratory. NREL/TP-5000- 75209.

Seroka, E. Fredj, J. Kohut, R. Dunk, T. Miles, and S. Glenn (2018), "Sea Breeze Sensitivity to Coastal Upwelling and Synoptic Flow Using Lagrangian Methods," *J. Geophys. Res. Atmos.*, vol. 123, no. 17, pp. 9443–9461, doi: 10.1029/2018JD028940.

Seroka, G., Dunk, R., and Fredj, E. (2019). "Analysis of Sea Breeze Types Using WRF and Lagrangian Methods". Aquawind, LLC. Available at: https://rucool.marine.rutgers.edu/downloads/publications/WRF%20Lagrangian%20Methods%20for%20Sea%20Breeze%20Types%20final.pdf

Seroka, G., Dunk, R., and Fredj, E. (2020). "Analysis of Sea Breeze Types using WRF and Lagrangian methods: Update using RU-WRF configuration". Aquawind, LLC. Available at: https://rucool.marine.rutgers.edu/wp-content/uploads/2020/10/WRF-Lagrangian-Methods-for-Sea-Breeze-Types_updateRUWRF_final.pdf

Sprenger, M. and H. Wernli (2015), "The LAGRANTO Lagrangian analysis tool – version 2.0," *Geosci. Model Dev.*, vol. 8, no. 8, pp. 2569–2586, doi: 10.5194/gmd-8-2569-2015.